Controlled Supramolecular Assembly of Helical Silica Nanotube–Graphene Hybrids for Chiral Transcription and Separation

Jong Hwa Jung,[†,*] Seung-Jin Moon,[†] Jinho Ahn,[†] Justyn Jaworski,[‡,*] and Seiji Shinkai[§,*]

[†]Department of Chemistry & Research Institute of Natural Science, Gyeongsang National University, Jinju 660-701, South Korea, [‡]Department of Chemical Engineering, Hanyang University, Seoul 133-791, South Korea, and [§]Institute for Advanced Study, Kyushu University, Fukuoka 819-0395, Japan

ABSTRACT Chiral templating and enantioselective separations are demonstrated on graphene surfaces as directed by encapsulated silica nanotubes. Electrostatic assembly of helical silica nanotubes within graphene sheets results in a hybrid material with the electrochemical properties of graphene and the capability for chiral recognition. Control of the silica nanotube helicity within the graphene hybrid provides a means for directed chiral templating of guest molecules on the outer graphene surface as revealed in the chiral transcription of N^1,N^3,N^5-tri(4-pyridinyl)cyclohexane-1,3,5-tricarboxamide as well as polyallylamine into supramolecular templated assemblies. Changing the helicity of the internal nanotube also provides control over enantiomer selectivity as demonstrated by the chiral separation of racemic mixtures of phenylalanine, tryptophan, and alanine derivatives.

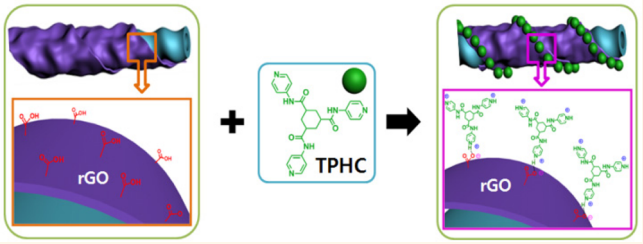

KEYWORDS: reduced graphene oxide · helical silica · chiral transcription · hybrid · nanotube

Over the years, researchers have explored chiral supramolecular architectures to further our understanding of nature's ability to create functional materials possessing the hierarchical structure over a range of size scales. The quest to control and predict supramolecular chirality of artificial systems remains an active topic for scientists, as chiral materials may offer unique functional approaches to sensing systems,[1−3] molecular memory systems,[4] and even asymmetric syntheses.[5−7] The creation of artificial chiral building blocks as well as chiral supramolecular assemblies has already demonstrated significant applicability to the selective detection and separation of chiral molecules and has provided a basis for transcription of novel chiral materials. The Yashima group, in particular, has produced prime examples of organic chiral materials for detection and amplification of chirality.[8,9] In addition, metal organic frameworks[10] and several other inorganic chiral materials have been created for optochiral applications and have shown exquisite structural control.[11−15] However, for inorganic chiral materials, there are few examples demonstrating the capability of supramolecular chiral transcription and recognition.[16,17] Our team has previously been the first to report right-handed and left-handed silica nanotubes (SNTs), prepared from chiral, self-assembled organogel templates.[18] Since then, several reports have demonstrated helical silica and mesoporous SNTs and fibers.[17−21] Che *et al.* have demonstrated that chiral mesoporous silica prepared from templated sol–gel reactions can control the molecular arrangement of asymmetric organic compounds.[16] This demonstration of chiral templating was found to be driven by electrostatic interactions between positive charges on the mesoporous silica and negative charges of the guest molecules. Most recently, Che's group and also Matsukizono *et al.* have shown that chiral silica can induce the chiral formation of nanoparticles within mesoporous silica and along silica walls.[16,17] These works have provided significant advances in the self-assembly of achiral molecules into

* Address correspondence to jonghwa@gnu.ac.kr, justynj@hanyang.ac.kr, shinkai_center@mail.cstm.kyushu-u.ac.jp.

Received for review December 28, 2012 and accepted March 1, 2013.

Published online March 01, 2013
10.1021/nn306006s

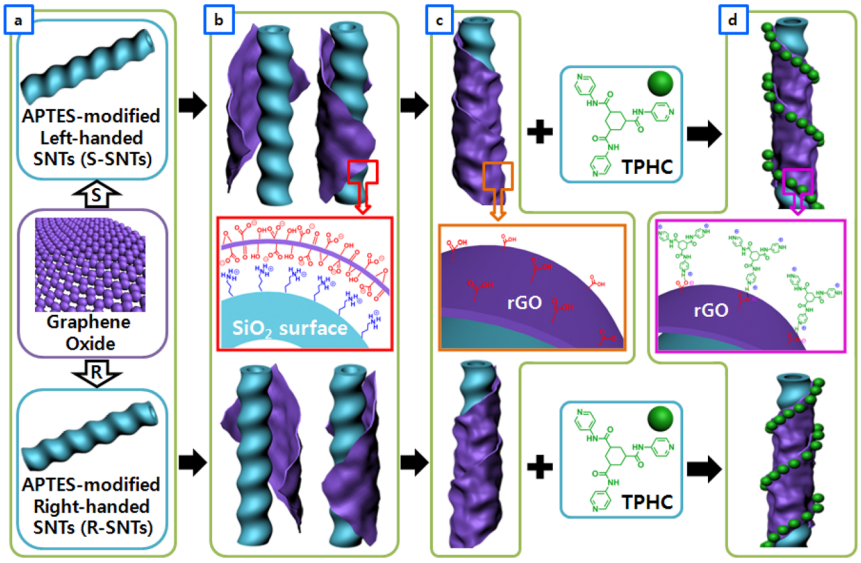

Figure 1. GO encapsulation of helical SNTs followed by reduction provides a hybrid material capable of enantioselective separation of molecules from mixtures as well as chiral molecular assembly of TPHC; (a) preparation of modified helical SNTs and GO, (b) wrapping of GO onto modified SNTs, (c) reduced GO hybrids with SNTs, and (d) chiral transcription of TPHC. Note: TPHC may not be limited to the edge of the rGO surface; SNTs have a diameter of ~100 nm and length of ~4 μm; GO has an area of ~0.55 μm^2.

chiral supramolecular complexes by use of inorganic materials.

An unfortunate drawback of such silica systems is the characteristically poor electrical and electrochemical properties. By graphene encapsulation of helical SNTs, we can introduce a number of remarkable physical, chemical, and electrical characteristics attributed to the graphene surface. The graphene-encapsulated helical SNTs revealed in this study would be particularly applicable to electronic and electrochemical chiral sensors.[22,23]

In addition, our work reveals an innovative advance in chiral transcription by showing that graphene encapsulation of helical SNTs can provide the appropriate surface characteristics necessary for the formation of chiral supramolecular assemblies using a variety of positively charged molecules. Since the surface properties of inorganic chiral materials may limit the type of molecule which can undergo chiral recognition, we show that by altering the surface characteristics through graphene encapsulation we may provide a surface amenable to chiral transcription of various molecules or polymer assemblies, as dictated by the helical sense of the underlying SNTs. We also provide the first report of using a graphene coating for helical SNTs in order to confer chiral recognition for enantioselective separation on the surface of graphene. These hybrid materials also exhibit excellent electrical properties, an advantageous characteristic for potential chiral sensor applications.

Herein, we provide details of our approach to enantioselective separation, as well as our strategy for creating supramolecular chiral assemblies on graphene, by demonstrating that chiral templates can be generated on left- or right-handed SNTs after encapsulated with reduce graphene oxide (rGO). By displaying positively charged amine modifications on the SNTs, we facilitate wrapping by negatively charged GO *via* proposed electrostatic driven assembly.[23,24] After chemical reduction, the rGO-encapsulated SNTs allow guest molecules to interact with the surface in a chiral manner dependent on the helical orientation of the interior silica. Specifically, we show that the positively charged guest molecule, N^1,N^3,N^5-tri(4-pyridinyl)cyclohexane-1,3,5-tricarboxamide (TPHC), could undergo chiral supramolecular assembly for the case of rGO-encapsulated helical silica but not for bare helical silica. The chiral templated material revealed tunable optical characteristics as controlled by the helicity of the SNT. In addition, the chiral material maintained electrical properties typical of those exhibited by rGO systems. This important finding opens the possibility for new chiral materials that possess the advantageous electrical, thermal, and mechanical properties of graphene combined with the functional capabilities afforded by chiral templating, including chiral recognition/separation and chiroptical properties as demonstrated in this system. Since our report reflects the first integration of rGO as a surface material component in chiral recognition and separation, it is important to clarify that it is the helicity of the internal SNT, rather than the rGO surface itself, that dictates the chiral selectivity of the system. It is, however, the surface of rGO that provides the essential complementary interactions for templating and separation to occur (Figure 1).

RESULTS AND DISCUSSION

To create the right- and left-handed helically structured SNTs used as the transcription directing element

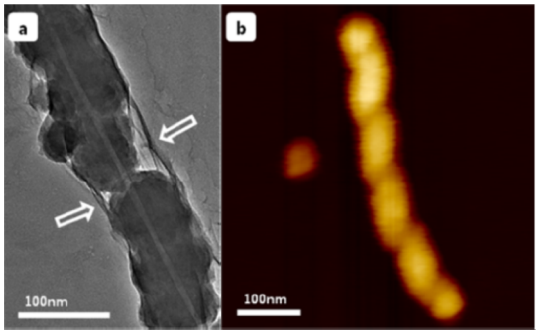

Figure 2. (a) TEM and (b) AFM images of rGO-encapsulated right-handed SNTs. The rGO sheet on the SNT is indicated by the arrows.

for chiral molecular templating, we employed our previously established sol−gel process incorporating chiral diaminocyclohexane-based organogels (Supporting Information Figure S1).[14,18,19] SEM and TEM images confirm the diameter of the helical SNTs to be 65−130 nm (Figures S2 and S3) with an average length of ~4 μm and a helical pitch ranging from 170 to 250 nm, while AFM images of GO reveal individual sheets having an approximate area of 0.55 μm^2 (Figures S3 and S4).

Modification of the helical SNTs was carried out using (3-aminopropyl)triethoxysilane (APTES) and confirmed from FT-IR spectra (Figure S5) by the enhancement of vibrational bands due to amino and methyl groups. This necessary modification provided a positively charged silica surface (Figure S6) for subsequent interaction with negatively charged graphene oxide (GO)[25,26] that had been prepared by Hummers' method for oxidative exfoliation.[26−29] Following coverage, the GO was reduced, providing chemically functionalized sheets containing hydroxyl, carbonyl, and carboxyl groups that could serve as coupling sites or chemical handles for subsequent templating reactions.[26,28,30]

In recent works, researchers have used graphene to enclose metal oxide nanoparticles for the purpose of energy storage applications,[24] revealing that encapsulation could be driven by electrostatic interactions. Similarly, encapsulation of silicon oxide nanoparticles by graphene was modeled to occur *via* a size-dependent summation of van der Waals forces[31] with experimental observation largely indicating electrostatic interactions.[23,32] Related work for a graphene coating within a carbon nanotube surface was evaluated using density functional theory methods wherein preferential elliptical or helical conformations were predicted due to key van der Waals attractions occurring at the edge.[33,34] Our study supports that the encapsulation of GO sheets onto SNTs is driven by surface electrostatics, based on our zeta-potential measurements revealing that opposite charges for APTES-modified silica and GO sheets correspond to aggregation behavior upon mixing in aqueous solution at or below pH 6.5, as seen in Figure S6. Using a suitable pH range (pH = 5.0), the electrostatic interaction induced assembly of GO around APTES-modified SNTs was readily achieved by simple mixing. After encapsulation followed by reduction of the GO-coated SNT with hydrazine treatment, the rGO samples were observed by TEM and AFM (Figure 2). As revealed in Figures 2 and S7, the AFM images demonstrate a helical structure with diameter of 69−135 nm. In addition, TEM and SEM images show that the modified SNTs were wrapped by rGO sheets, which was further confirmed by using a TEM technique for elemental mapping (Figure S8). XPS analysis of the hybrid material, consisting of carbon, silicon, and oxygen, demonstrated a distinct increase in the representative carbon (Figures 2 and S9, Tables S1 and S2), thereby confirming the presence of rGO on both right- and left-handed SNTs. The APTES-modified right-handed silica nanotube without graphene consists of 30.87% for Si, 59.10% of O, 8.31% for C, and 1.33% for N. After enclosure of the modified right-handed SNTs by rGO, the hybrid was found to consist of 23.09% for Si, 46.39% for O, 28.20% for C, and 2.31% for N. This clear increase in carbon content is believed to be due to enclosure by rGO. Furthermore, high-resolution Raman spectroscopy (Figure S10) of the hybrid revealed two characteristic rGO peaks: the G band at ~1602 cm^{-1} and D band at ~1352 cm^{-1}. According to thermal gravimetric analysis (TGA) measurements (Figure S11), 23.2 wt % of carboxyl group exists on the surface of rGO.

To assess if our hybrid material maintains the functional properties of graphene, we initially examined its conductive capabilities. As confirmed by cyclic voltammetry (Figure S12), the rGO-encapsulated SNTs exhibited comparable electrical properties to the reduced graphene oxide electrode material (superior to GO and KCl), indicating that such properties of rGO were preserved in the hybrid material. Similar materials with graphene have typically exhibited this characteristic form of rectangular curve without distinct redox peaks.[35] Given that rGO encapsulation of the SNTs did not affect the beneficial electrical properties of graphene in the hybrid, the potential remains for its integration with electronic systems.

Our hybrid material revealed an interesting property attributed to the helical SNTs. Specifically, hybrids containing core right- or left-handed SNTs were found to be capable of distinct chiral transcription of guest molecules into supramolecular templated assemblies, while bare SNTs could not. For chiral transcription of TPHC as directed by the helical sense of the underlying SNT, the positive surface charge of APTES-modified SNT was first mitigated by wrapping of negatively charged GO followed by chemical reduction (Figure S6, Tables S1 and S2). The resulting hybrid displays a more negative surface charge with structural helicity, as well as complementary sites for interaction with positively charged pyridine groups, to facilitate stabilization of a TPHC supramolecular chiral assembly.

The Raman spectrum of the L-SNTs/r-GO hybrid displays two prominent peaks at 1357.4 and 1600.7 cm^{-1}, corresponding to the well-documented D and G bands, respectively (Figure S13). The G mode is related to the vibration of sp^2-hybridized carbon. The phonon mode at 1357.4 cm^{-1}, also known as the D mode, corresponds to the conversion of an sp^2-hybridized carbon to an sp^3-hybridized carbon. For pure TPHC, its spectrum shows bands at 663.2, 992.5, and 1214.5 cm^{-1} corresponding to C−H out-of-plane mode, −CN═C− stretching, and −C−H in-plane mode vibration of the pyridine moiety, respectively.[36,37] For the Raman spectrum of TPHC loaded onto rGO-encapsulated L-silica nanotubes, it closely represents the superposition of Raman spectra from individual graphene and TPHC samples, indicating the presence of both components in the hybrid. In addition, compared with the Raman bands of TPHC alone, there is a clear red shift in the peaks of TPHC loaded onto rGO-encapsulated L-silica nanotubes for the stretching vibrations of the C−H out-of-plane mode and −CN═C− stretching in the pyridine moiety at 658.5 and 988.2 cm^{-1}, respectively. Also, the peak at 1207.6 cm^{-1} due to the C−H in-plane mode vibration of the pyridine moiety was red-shifted compared to 1214.5 cm^{-1} for pure TPHC. The spectral red shift phenomena of the TPHC loaded onto rGO-encapsulated L-silica nanotubes might be attributed to the favorable $\pi-\pi$ interaction between graphene sheets and the TPHC backbone.[36−41]

In addition to the red shift phenomenon observed in Raman spectra after TPHC exposure, subsequent observations in the solid-state diffuse reflectance circular dichroism (DRCD) spectrum provide confirmation that TPHC undergoes chiral assembly on the rGO-wrapped SNTs. Specifically, TPHC assembled on the reduced GO−silica hybrid revealed a direct correlation between the helicity of the SNT and the arrangement of the TPHC on the surface. The λ_{max} value of TPHC in the UV absorption spectrum appears at 245 nm, which corresponds to the $\lambda_\theta = 0$ values in the CD spectra (Figure 3A). The TPHC assemblies formed on the rGO hybrids with right-handed SNTs produced a negative first Cotton effect (Figure 3A,a), indicating a counterclockwise orientation of dipole moments in the supramolecular assembly. In contrast, the DRCD spectrum of TPHC assembled on the rGO hybrids with left-handed SNTs revealed a positive first Cotton effect (Figure 3A,b). These findings indicate that the hybrids provoked chiral transcription of TPHC molecules on the graphene surface as determined by the helical sense of the internal silica. Control experiments showed no CD response for the individual TPHC solution or rGO with TPHC (Figure S17). In addition, no CD response was observed for unmodified or APTES-modified SNTs exposed to TPHC (Figure S14), due to their very weak acidity and positive charge, respectively. This important point reveals a novel transcription mechanism in which the SNTs require rGO encapsulation in order to elicit chiral transcription of the TPHC molecules, as observed from CD spectra.

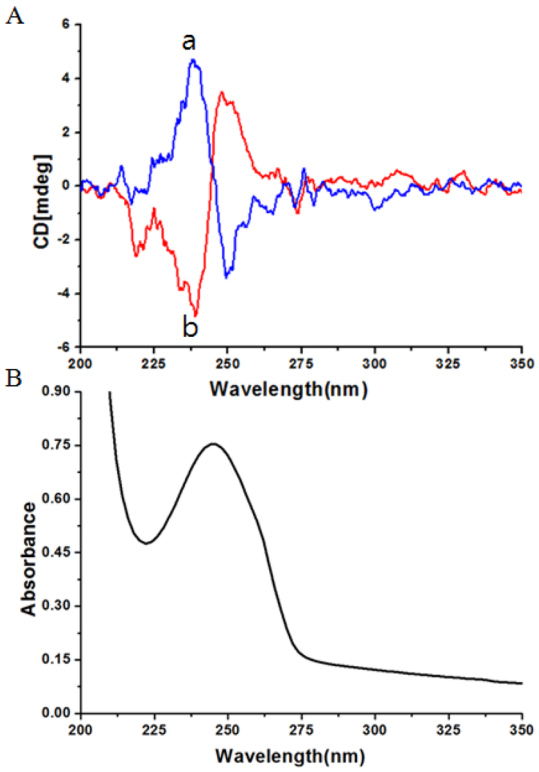

Figure 3. (A) DRCD spectra of TPHC loaded onto rGO-encapsulated (a) R- and (b) L-SNTs at pH 5.0. (B) UV absorption spectrum of TPHC.

In addition to TPHC, right- and left-handed chiral transcription of polyallylamine (PAA) was also achieved using r-GO hybrids (Figure S15). PAA loaded onto rGO hybrids with R-SNTs revealed CD spectra with a negative first Cotton effect in the UV/vis absorption region owing to the polymer main chain, indicating that the adsorbed PAA exhibited a chiral formation. In comparison, PAA loaded onto rGO with L-SNTs showed CD signals in these regions, revealing a positive first Cotton effect, implying that the main chain exists in an antipodal chiral conformation to that obtained from R-SNTs. Direct chiral transcription of other guest molecules on graphene surfaces may be useful for various chiral technologies including enantioselective separation or recognition.

To explore the potential of this hybrid material for chiral recognition, the helically distinct forms of graphene-wrapped silica were separately incubated with racemic mixtures of enantiomers for several amino acid derivatives (Figures 4 and S16). Specifically, rGO-encapsulated L-SNTs were incubated with each of a 1:1 mixture of L and D form derivatives of phenylalanine, tryptophan, and alanine. The mixtures were filtered to capture the solid product of left-handed rGO-SNTs along with any bound amino acid derivative. By observing the CD spectra of the filtered mixture, we could quantify the amount of adsorbed amino acid (Table S3).

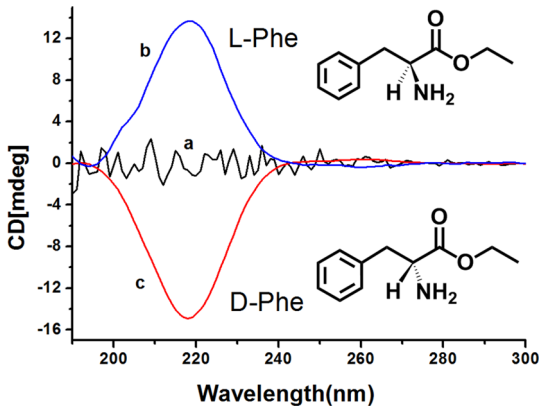

Figure 4. (a) DRCD of samples containing 1:1 mixtures of L- and D-phenylalanine derivatives. After incubation of rGO-SNTs with samples containing 1:1 mixtures of L- and D-phenylalanine derivatives in pH 5.0 aqueous solution, the solid product was filtered, and the DRCD spectra of rGO-encapsulated (b) L-SNTs showed selective adsorption of L-phenylalanine while rGO-encapsulated (c) R-SNTs showed selective adsorption of D-phenylalanine.

For assembly of amino acids, among other biomolecules, on nanostructured surfaces, it has previously been revealed that CD offers an effective analytical technique for examining chiral separation and templating.[42,43] From our observations of the CD spectra, we found the left-handed rGO-SNTs to selectively capture the L form (L-Phe, L-Trp, or L-Ala) amino acid derivative, thereby removing it from solution phase. Analogously, right-handed rGO-SNTs were found to bind selectively with the D form amino acid derivatives allowing them to be separated from the solution phase. The CD spectrum in Figure 4b provides an example that the L form of the Phe derivative has remained after filtration by binding with the left-handed rGO-SNT hybrids (indicated in blue). Contrastingly, racemic mixtures incubated with rGO-encapsulated R-SNTs can be seen to bind the D-Phe derivative enantiomer, as seen by the red CD spectrum in Figure 4c. This is similarly observed for the cases of Ala and Trp derivatives (Figure S16), thereby providing evidence of a generalized behavior in which the chiral templating capabilities of rGO surfaces with interior left- or right-handed SNTs can impose clear enantioselective recognition for L or D forms of amino acid derivatives, respectively (Table S3 and Figure S16). The role of rGO in providing a negatively charged surface with complementary sites for interaction with positively charged amines on the Phe, Trp, and Ala derivatives may help to stabilize their supramolecular assembly in a similar manner to the case observed for pyridine groups on TPHC. In contrast, the amino acid derivatives preferentially adsorbed to either the L or R helical form of the rGO-SNT hybrids for L or D enantiomers, respectively, while the achiral TPHC could be templated onto either helical form of the hybrid. This approach is distinct from that of general chiral organic derivatives that have already been widely developed for separating enantiomeric mixtures using chromatography. So far, there are no reports on the use of an inorganic material for direct chiral separation by chiral adsorption of enantiomeric mixtures using an achiral surface group as the chiral selector.

CONCLUSIONS

In summary, we have found that helical silica nanotubes can be encapsulated with rGO to provide a hybrid material capable of the chiral transcription of organic components onto its surface. In addition, we are the first to reveal enantioselective separation using an achiral surface as governed by the helical sense of a SNT interior. While other research groups have shown enantioselectivity with chiral forms of silica[44] or even chiral supramolecular assembly,[16,45] our work provides the first demonstration that such enantioselectivity and chiral transcription can be implemented with graphene surfaces. Aside from showing the capability of this material in chiral separation systems, the prospective of enantioselective recognition may be valuable for sensing applications. The fact that this hybrid exhibits electrochemical properties similar to pure rGO is especially beneficial for use in sensor development. We suspect the important findings provided in this work may open the way for diverse chiral applications outside of sensing and separation as we expect other research areas may take advantage of the unique integration of chiral templates onto graphene.

METHODS

General Considerations. All other chemicals were purchased from Aldrich, TCI, or Wako and used as received. ^{1}H and ^{13}C NMR spectra were measured on a Bruker ARX 300 apparatus. IR spectra were obtained for KBr pellets, in the range of 400−4000 cm^{-1}, with a Shimadzu FT-IR 8400S instrument, and transmission electron microscopy (TEM) images were taken with a JEOL JEM-2100 F instrument operated at 50 keV. Images were recorded on 2k CCD (Gatan Inc. USC 1000). Mass spectra were obtained by a JEOL JMS-700 mass spectrometer. AFM analysis was performed in a noncontact mode under the following condition: scan rate of 1.0 Hz; PPP-NCHR 10 M cantilever (Park systems). Cyclic voltammetric analysis was performed by using a BASi C3 EF-1085 cell stand with samples coated onto a polished GC electrode in 1.0 M KCl solution with a carbon counter electrode and a Ag/AgCl reference electrode.

Graphene Oxide (GO). GO was prepared from natural graphite (Sigma-Aldrich) using a modified Hummers' method.[27] In a typical reaction, 1.00 g of graphite, 1.00 g of $NaNO_3$, and 50 mL of H_2SO_4 were stirred in an ice bath for 30 min. Following, 8.00 g of $KMnO_4$ was slowly added. The solution was transferred to a 35 °C water bath and stirred for about 2 h to form a thick green paste. After that, the mixture was stirred for 3 days at room temperature. Then, 80 mL of water was added very slowly followed by stirring for 1 h while the temperature was increased to ~90 °C. Finally, 200 mL of water was added followed by the slow addition of 20 mL of H_2O_2 (30%), turning the color of the solution from dark brown to a pale brown yellowish. The warm solution was then filtered and washed with water. GO solution (~0.2 wt %) was ultrasonicated for 1 h, and

the remaining non-exfoliated GO was removed by centrifugation at 14 000 rpm (20 817 rcf) for 30 min. The solution was then membrane filtered. The final product was then stored under vacuum for drying.

Preparation of APTES-Modified Helical Silica Nanotubes. The obtained silica templates (0.5 g) were further dispersed into 50 mL of dry toluene solution *via* sonication. After 30 min, 0.5 mL of (3-aminopropyl)triethoxysilane was poured into the above solution and refluxed for 24 h under argon atmosphere to obtain APTES-modified silica nanotemplates.

Synthesis of N^1,N^3,N^5-Tri(4-pyridinyl)cyclohexane-1,3,5-tricarboxamide (TPHC). A solution of cyclohexane-1,3,5-tricarboxylic acid (0.5 g, 2.313 mmol), TEA (1.00 mL, 7.00 mmol), and $SOCl_2$ (15 mL, 69.35 mmol) along with dry DMC (20 mL) was incubated in an ice bath. The reaction mixture was stirred for 22 h in the ice bath and then heated for 2 h under reflux. After being cooled to room temperature, solvents were removed from the reaction mixture to give a yellowish-white waxy solid. Next, 4-aminopyridine (0.87 g, 9.245 mmol) and TEA (1.00 mL, 7.00 mmol) in dry THF (20 mL) were added dropwise to the reaction mixture and stirred for 24 h under reflux. After cooling to room temperature, the reaction mixture was filtered, and the filtrate was washed with THF and methanol solutions (0.2 g, yield 20%): mp = 312 °C, ^{1}H NMR (300 MHz, DMSO-d_6) δ 8.40 (d, 6H), 7.69 (d, 6H), 2.67 (m, 3H), 2.18 (m, 3H), 1.86 (m, 3H); ^{13}C NMR (75 MHz, DMSO-d_6) δ 174.4, 150.8, 146.1, 113.8, 44.0, 31.1; IR (KBr, cm^{-1}) 3500, 3257, 3171, 3079, 2998, 1691, 1594, 1513, 1330, 1174, 825; HRMS (FAB) $[M + H]^+$ m/z = 445.1993 (calcd M_w = 444.1910). Anal. Calcd for $C_{24}H_{24}N_6O_3$: C, 64.85; H, 5.44; N, 18.91. Found: C, 64.68; H, 5.45; N, 18.89.

Graphene Oxide Encapsulation of Silica Nanotubes. Graphene-encapsulated oxides were fabricated *via* the electrostatic interaction between positively charged APTES-modified oxides and negatively charged graphene oxide in aqueous solutions. In a typical process, 20 mL of APTES-modified silica dispersion (0.5 mg mL^{-1}) was added into a 30 mL aqueous graphene oxide suspension (0.05 mg mL^{-1}) under mild magnetic stirring. After 1 h, 0.5 mL of hydrazine (35 wt %) was added into the above suspension to reduce graphene oxide. The solution was membrane filtered and washed with water.

Templated Assembly of TPHC. Five milligrams of TPHC was dissolved in 5 mL of ion-exchanged, degassed water with stirring for 5 min at room temperature (pH = 5.0). Then, 50 mg of rGO composite (left- or right-handed silica nanotubes encapsulated with reduced grapheme oxides) was dispersed in the above solution with stirring for 20 min at room temperature. The solid was separated with a centrifuge and dried in air at 313 K.

Separation of L and D Form Amino Acid Enantiomers. For separation of L and D forms, the graphene-encapulated R-silica or S-silica (10.0 mg) was added to a mixture of L and D form amino acids derivatives (1:1 v/v, 1.0 mM) in water (pH = 5.0). The mixtures were stirred for 30 min and filtered. The remaining solid product containing any bound amino acid derivatives after filtration was quantified by solid-state diffuse reflectance circular dichroism (DRCD).

D- and L-Phenylalanine Ethyl Ester (D- and L-Phe). A solution of phenylalanine (1.00 g, 6.06 mmol) and $SOCl_2$ (3.90 mL, 5.30 mmol) was placed in dry EtOH (27 mL) and was incubated in an ice bath. The reaction mixture was stirred for 1 h in the ice bath and then refluxed for 24 h. After being cooled to room temperature, the solvents were removed from the reaction mixture. The product was then extracted into MeCN. The solution was filtered, and the filtrate was concentrated under reduced pressure to give a white product. Then, the product was recrystallized in MeCN/ethanol (1.00 g, yield 86%): mp = 155 °C; ^{1}H NMR (300 MHz, DMSO-d_6) δ 8.93 (s, 3H), 7.40 (m, 5H), 4.16 (q, 1H), 4.07 (m, 2H), 3.31 (q, 1H), 3.07 (q 1H), 1.17 (t, 3H); ^{13}C NMR (75 MHz, DMSO-d_6) δ 168.76, 133.11, 129.94, 129.42, 128.69, 62.54, 55.84, 35.83 14.28; IR (KBr, cm^{-1}) 2914, 2862, 2639, 2483, 1741, 1503, 1461, 1238, 1218, 748, 706; MS $[M + H]^+$ m/z = 194.11 (calcd M_w = 193.11). Anal. Calcd for $C_{24}H_{24}N_6O_3$: C, 68.37; H, 7.82; N, 7.25. Found: C, 67.57; H, 7.80; N, 7.22.

D- and L-Alanine Methyl Ester (D- and L-Ala) and D- and L-Tryptophan Alanine Methyl Ester (D- and L-Trp). These amino acid derivatives were purchased from Sigma Aldrich.

Conflict of Interest: The authors declare no competing financial interest.

Acknowledgment. This work was supported by a grant from World Class Project (WCU) supported by Ministry of Education Science and Technology (R32-2008-000-20003-0) and NRF (2012R1A4A1027750), Korea. In addition, this work was partially supported by a grant from the Next-Generation BioGreen 21 Program (SSAC, Grant No. PJ009041022012), Rural Development Administration, Korea.

Supporting Information Available: XPS, SEM, TEM, AFM, TGA, FT-IR, and Raman spectra characterization in addition to DRCD spectra of control samples, zeta-potential measurements, and detailed experimental methods. This material is available free of charge *via* the Internet at http://pubs.acs.org.

REFERENCES AND NOTES

1. Mathew, B.; Kuboyam, T.; Nakamura, S.; Takagi, M. Lipophilic Peptide as Novel Sensory Material for Chiral Amine Recognition. *Chem. Lett.* **2000**, *29*, 1026–1027.
2. Du, Y.; Guo, S.; Qin, H.; Dong, S.; Wang, E. Target-Induced Conjunction of Split Aptamer as New Chiral Selector for Oligopeptide on Graphene−Mesoporous Silica−Gold Nanoparticle Hybrids Modified Sensing Platform. *Chem. Commun.* **2012**, *48*, 799–801.
3. Hongqing, C.; Jiaxi, C.; Anhua, L.; Xinhua, W. Synthesis and Helix-Sense-Selective Polymerization of Chiral Vinyl Biphenyl Monomers. *Acta Polym. Sin.* **2010**, *2*, 15–15.
4. De Jong, J. J.; Lucas, L. N.; Kellogg, R. M.; van Esch, J. H.; Feringa, B. L. Reversible Optical Transcription of Supramolecular Chirality into Molecular Chirality. *Science* **2004**, *304*, 278–281.
5. Walkup, R. D.; Cole, D. C.; Whittlesey, B. R. Silicon-Containing Amino Acids and Peptides. Asymmetric Synthesis of (Trialkylsilyl) Alanines. *J. Org. Chem.* **1995**, *60*, 2630–2634.
6. Lou, L.; Peng, X.; Yu, K.; Liu, S. Asymmetric Hydrogenation of Acetophenone Catalyzed by Chiral Ru Complex in Mesoporous Material Supported Ionic Liquid. *Catal. Commun.* **2008**, *9*, 1891–1893.
7. Garcia, R. A.; Gricken, R. V.; Iglesias, J.; Morales, V.; Gordillo, D. Synthesis of Chiral Periodic Mesoporous Silicas Incorporating Tartrate Derivatives in the Framework and Their Use in Asymmetric Sulfoxidation. *Chem. Mater.* **2008**, *20*, 2964–2971.
8. Goto, H.; Yashima, E. Electron-Induced Switching of the Supramolecular Chirality of Optically Active Polythiophene Aggregates. *J. Am. Chem. Soc.* **2002**, *124*, 7943–7949.
9. Yashima, E.; Maeda, K.; Okamoto, Y. Memory of Macromolecular Helicity Assisted by Interaction with Achiral Small Molecules. *Nature* **1999**, *399*, 449–451.
10. Sun, C. Y.; Qin, C.; Wang, C. G.; Su, Z. M.; Wang, S.; Wang, X. L.; Yang, G. S.; Shao, K. Z.; Lan, Y. Q.; Wang, E. B. Chiral Nanoporous Metal-Organic Frameworks with High Porosity as Materials for Drug Delivery. *Adv. Mater.* **2011**, *23*, 5629–5632.
11. Hodgkinson, I.; Wu, Q. H. Inorganic Chiral Optical Materials. *Adv. Mater.* **2001**, *13*, 889–897.
12. Jiang, X. M.; Zhang, M. J.; Zeng, H. Y.; Guo, G. C.; Huang, J. S. Inorganic Supramolecular Compounds with 3-D Chiral Frameworks Show Potential as Both Mid-IR Second-Order Nonlinear Optical and Piezoelectric Materials. *J. Am. Chem. Soc.* **2011**, *133*, 3410–3418.
13. Yokoi, T.; Ogawa, K.; Lu, D.; Kondo, J.; Kubota, Y.; Tatsumi, T. Preparation of Chiral Mesoporous Materials with Helicity Perfectly Controlled. *Chem. Mater.* **2011**, *23*, 2014–2016.
14. Xia, Y.; Zhou, Y.; Tang, Z. Chiral Inorganic Nanoparticles: Origin, Optical Properties and Bioapplications. *Nanoscale* **2011**, *3*, 1374–1382.
15. Jung, J. H.; Park, M.; Shinkai, S. Fabrication of Silica Nanotubes by Using Self-Assembled Gels and Their Applications in Environmental and Biological Fields. *Chem. Soc. Rev* **2010**, *39*, 4286–4302.

16. Qiu, H.; Inoue, Y.; Che, S. Supramolecular Chiral Transcription and Recognition by Mesoporous Silica Prepared by Chiral Imprinting of a Helical Micelle. *Angew. Chem., Int. Ed.* **2009**, *48*, 3069–3072.
17. Matsukizono, H.; Jin, R. H. High-Temperature-Resistant Chiral Silica Generated on Chiral Crystalline Templates at Neutral pH and Ambient Conditions. *Angew. Chem., Int. Ed.* **2012**, *24*, 5862–5865.
18. Jung, J. H.; Ono, Y.; Hanabusa, K.; Shinkai, S. Creation of Both Right-Handed and Left-Handed Silica Structures by Sol−Gel Transcription of Organogel Fibers Comprised of Chiral Diaminocyclohexane Derivatives. *J. Am. Chem. Soc.* **2000**, *122*, 5008–5009.
19. Moreau, J. E.; Vellutini, L.; Man, M. W. C.; Bied, C. New Hybrid Organic−Inorganic Solids with Helical Morphology *via* H-Bond Mediated Sol−Gel Hydrolysis of Silyl Derivatives of Chiral (*R*,*R*)- or (*S*,*S*)-Diureidocyclohexane. *J. Am. Chem. Soc.* **2001**, *123*, 1509–1510.
20. Che, S.; Liu, Z.; Ohsuna, T.; Sakamoto, K.; Terasaki, O.; Tatsumi, T. Synthesis and Characterization of Chiral Mesoporous Silica. *Nature* **2004**, *429*, 281–284.
21. Chen, Y.; Li, B.; Wu, X.; Zhu, X.; Suzuki, M.; Hanabusa, K.; Yang, Y. Hybrid Silica Nanotubes with Chiral Walls. *Chem. Commun.* **2008**, 4948–4950.
22. Han, T. H.; Lee, W. J.; Lee, D. H.; Kim, J. E.; Choi, E.-Y.; Kim, S. O. Peptide/Graphene Hybrid Assembly into Core/Shell Nanowires. *Adv. Mater.* **2010**, *22*, 2060–2064.
23. Myung, S.; Solanki, A.; Kim, C.; Park, J.; Kim, K. S.; Lee, K. B. Graphene-Encapsulated Nanoparticle-Based Biosensor for the Selective Detection of Cancer Biomarkers. *Adv. Mater.* **2011**, *23*, 2221–2225.
24. Yang, S.; Feng, X.; Ivanovici, S.; Müllen, K. Fabrication of Graphene-Encapsulated Oxide Nanoparticles: Towards High-Performance Anode Materials for Lithium Storage. *Angew. Chem., Int. Ed.* **2010**, *49*, 8408–8411.
25. Zhou, X.; Huang, X.; Qi, X. Y.; Wu, S. X.; Xue, C.; Boey, F.; Yan, Q.; Chen, P.; Zhang, H. *In Situ* Synthesis of Metal Nanoparticles on Single-Layer Graphene Oxide and Reduced Graphene Oxide Surfaces. *J. Phys. Chem. C* **2009**, *113*, 10842–10846.
26. Li, D.; Muller, M. B.; Gilje, S.; Kaner, R. B.; Wallace, G. G. Processable Aqueous Dispersions of Graphene Nanosheets. *Nat. Nanotechnol.* **2008**, *3*, 101–105.
27. Hummers, W. S.; Offeman, R. E. Preparation of Graphitic Oxide. *J. Am. Chem. Soc.* **1958**, *80*, 1339–1339.
28. Liang, Y. Y.; Frisch, J.; Zhi, L. J.; Norouzi-Arasi, H.; Feng, X. L.; Rabe, J. P.; Koch, N.; Müllen, K. Transparent, Highly Conductive Graphene Electrodes from Acetylene-Assisted Thermolysis of Graphite Oxide Sheets and Nanographene Molecules. *Nanotechnology* **2009**, *20*, 434007.
29. Bai, H.; Li, C.; Shi, G. Functional Composite Materials Based on Chemically Converted Graphene. *Adv. Mater.* **2011**, *23*, 1089–1115.
30. Oh, J.; Lee, J. H.; Koo, J. C.; Choi, H. R.; Lee, Y.; Kim, T.; Luong, N. D.; Nam, J. D. Graphene Oxide Porous Paper from Amine-Functionalized Poly(glycidyl methacrylate)/Graphene Oxide Core−Shell Microspheres. *J. Mater. Chem.* **2010**, *20*, 9200–9204.
31. Xia, D.; Xue, Q.; Xie, J.; Chen, H.; Lv, C. Silicon/Graphene Core/Shell Nanowires Produced by Self-Scrolling. *Comput. Mater. Sci.* **2010**, *49*, 588–592.
32. Luo, F.; Chen, L.; Ning, N.; Wang, K.; Chen, F.; Fu, Q. Interfacial Enhancement of Maleated Polypropylene/Silica Composites Using Graphene Oxide. *J. Appl. Polym. Sci.* **2012**, *125*, E348–E357.
33. Talyzin, A. V.; Anoshkin, I. V.; Krasheninnikov, A. V.; Nieminen, R. M.; Nasibulin, A. G.; Jiang, H.; Kauppinen, E. I. Synthesis of Graphene Nanoribbons Encapsulated in Single-Walled Carbon Nanotubes. *Nano Lett.* **2011**, *11*, 4352–4356.
34. Lebedeva, I. V.; Popov, A. M.; Knizhnik, A. A.; Khlobystov, A. N.; Potapkin, B. V. Chiral Graphene Nanoribbon Inside a Carbon Nanotube: *Ab Initio* Study. *Nanoscale* **2012**, *4*, 4522–4529.
35. Lee, Y. R.; Song, M.; Lee, K. M.; Kim, I. Y.; Hwan, S. Synthesis and Electrochemical Characterization of Reduced Graphene Oxide-Manganese Oxide Nanocomposites. *J. Electrochem. Sci. Technol.* **2011**, *2*, 1–7.
36. Luo, J.; Jing, S.; Wu, Y.; Chen, M.; Liu, X. Synthesis of Stable Aqueous Dispersion of Graphene/Polyaniline Composite Mediated by Polystyrene Sulfonic Acid. *J. Polym. Sci., Polym. Chem.* **2012**, *50*, 4888–4894.
37. King, R. C. Y.; Roussel, F.; Brun, J.-F.; Gors, C. Carbon Nanotube-Polyaniline Nanohybrids: Influence of the Carbon Nanotube Characteristics on the Morphological, Spectroscopic, Electrical and Thermoelectric Properties. *Synth. Met.* **2012**, *162*, 1348–1356.
38. Gaff, J.; Franzen, S. Resonance Raman Enhancement of Pyridine on Ag Clusters. *Chem. Phys.* **2012**, *397*, 34–41.
39. Wu, D. Y.; Ren, B.; Jiang, Y. X.; Xu, X.; Tian, Z. Q. Density Functional Study and Normal-Mode Analysis of the Bindings and Vibrational Frequency Shifts of the Pyridine−M (M = Cu, Ag, Au, Cu+, Ag+, Au+, and Pt) Complexes. *J. Phys. Chem. A* **2002**, *106*, 9042–9052.
40. Naumenko, A.; Yashchuk, V.; Bliznyuk, V.; Singamaneni, S. Peculiarities of Raman Spectra of Polyurethane/Carbon Nanotube Composite. *Eur. Phys. J. B* **2012**, *85*, 120–126.
41. Jensen, L.; Aikensb, C. M.; Schatzc, G. C. Electronic Structure Methods for Studying Surface-Enhanced Raman Scattering. *Chem. Soc. Rev.* **2008**, *37*, 1061–1073.
42. Li, Z.; Zhu, Z.; Liu, W.; Zhou, Y.; Han, B.; Gao, Y.; Tang, Z. Reversible Plasmonic Circular Dichroism of Au Nanorod and DNA Assemblies. *J. Am. Chem. Soc.* **2012**, *134*, 3322–3325.
43. Zhu, Z.; Liu, W.; Li, Z.; Han, B.; Zhou, Y.; Gao, Y.; Tang, Z. Manipulation of Collective Optical Activity in One-Dimensional Plasmonic Assembly. *ACS Nano* **2012**, *6*, 2326–2332.
44. Paik, P.; Gedanken, A.; Mastai, Y. Enantioselective Separation Using Chiral Mesoporous Spherical Silica Prepared by Templating of Chiral Block Copolymers. *ACS Appl. Mater. Interfaces* **2009**, *1*, 1834–1842.
45. Li, C.; Deng, K.; Tang, Z.; Lei, J. Twisted Metal−Amino Acid Nanobelts: Chirality Transcription from Molecules to Frameworks. *J. Am. Chem. Soc.* **2010**, *132*, 8202–8209.